Enhancement of Gas Sensing Performance of Iron Oxide Lignin/Polyvinyl Alcohol Nanocomposite Films

Firdous M. Mahmood [1]
Mazin A. Alalousi [2]
Abbas H. Faris [3]

[1] Department of Physics, College of Science, University of Anbar, Ramadi, IRAQ
[2] Nanomaterials Research Center, University of Anbar, Ramadi, IRAQ
[3] Department of Chemical and Petrochemical Engineering, College of Engineering, University of Anbar, Ramadi, IRAQ

The current study investigates the structural properties of lignin/polyvinyl alcohol composite films with particular reference to the impact of Fe_2O_3 loading and carbonization toward CO_2 gas sensor usage. The prepared films showed the dominance of the C_4 phase, even though the concentration of Fe_2O_3 nanoparticles in the films was important in establishing their properties. Morphological variations with the content of Fe_2O_3 were observed using field-emission scanning electron microscopy (FE-SEM), from spherical agglomerates to fibrous morphology and nanorods. Maintenance by various concentrations of Fe_2O_3 of various functional groups, like hydroxyl and aromatics, was established by using Fourier transform infrared (FTIR) spectroscopy. Enhanced CO_2 sensitivity in the instance of measurements of gases was shown with the best performance at the 4-ppm concentration of Fe_2O_3. These results demonstrate the utilization of carbon nanomaterials synthesized from lignin as active, environmentally friendly gas sensors.

Keywords: Biopolymer; Iron oxide; Nanocarbon rods; Gas sensors
Received: 4 April 2025; **Revised:** 21 May 2025; **Accepted:** 28 May 2025

1. Introduction

Emerging technological advancements are needed to address global challenges like environmental pollution and growing demands for impactful solutions. It takes advanced process optimization systems capable of monitoring the environmental conditions, infrastructure, and process efficiency to increase output while lowering pollution [1]. For the detection of gas molecules, heavy metals, humidity, biomolecules, toxins, pH, pressure, and other substances, there are a wide variety of sensors that exist today. However, the majority of these sensors have poor limits of detection (LOD), low sensitivity or selectivity, excessively slow response times, and sometimes even require pretreatment. While advanced process optimization systems offer potential benefits, they can also be prohibitively expensive and complex to implement, especially for smaller operations. Additionally, reliance on technology may overlook simpler, more cost-effective methods that could achieve similar environmental goals without the drawbacks of sophisticated sensors. Most importantly, they have limitedly [2]. Carbon nanomaterials play a critical role in sensing, pharmaceuticals, and controlled drug deliveries [3]. Fullerenes (zero-dimensional CNMs like C60) consist of pentagon-containing carbon structures, resembling buckled graphene sheets rolled into spheres. Comprising 30 to 300 carbon atoms, they are among the most extensively studied CNMs, particularly in electrochemical sensor devices. Graphene, alternatively, is a two-dimensional sheet of carbon atoms with sp^2 atoms. Graphene sheets rolled up give rise to either single-walled or multi-walled carbons [4].

CNMs enhance sensor performance due to their tunable electrical properties and high sensitivity. Various analytes were successfully detected using CNMs-based sensors that have beaten traditional sensing technologies in performance, seeking better sensitivity [5]. Growing concerns over environmental sustainability and declining petroleum resources have spurred research into green, biodegradable alternatives and naturally available resources. Ganesan et al. prepared self-assembled multifunctional carbon quantum dots (CQDs) via direct pyrolysis combined with microwave-assisted synthesis using Ziziphus mauritiana stone biomass (as a bioresource precursor). The CQDs demonstrated effective fluorescence for the selective and sensitive detection (sensor) of NH_3 with a detection limit of 10 nmol for the concentration of NH_3 in aquatic environment samples [6]. Šafranko et al. presented a facile hydrothermal approach to prepare CQDs derived from biomass from citrus peel and amino acids. The gradual increase in N content (amino acids) increased the quantum yield of the synthesized CQDs. The prepared CQDs showed good biocompatibility, stability in aqueous and high ionic strength media, and similar optical properties. The results obtained showed a selective response towards Fe^{3+} detection [7]. Additionally, lignin is a promising alternative for sustainable material production. It is ranked as the second most abundant natural material after cellulose, thanks to its unique composition and

adaptability to diverse applications. In recent years, extensive research efforts have been directed towards exploiting lignin as an active raw material for carbon fiber (CF) production due to its high content of aromatic ring structural units, making it an ideal source for carbon materials [8]. As well, carbon nanospheres are advanced materials with promising potential in multiple fields, as they are one of the key components of the carbon family of materials with wide applications [9]. This project aims to develop carbon nanorod films and assess their gas-sensing performance.

2. Materials and Method

Lignin powder was extracted from date palm tree waste by a chemical treatment. Initially, the sawdust was dissolved in a sodium hydroxide (NaOH) solution with a concentration of 10%, maintaining a solid-to-solvent ratio of 1:10. The mixture was heated to 150°C for three hours to extract lignin. Next, the solution was filtered using filter paper to remove insoluble residues. The lignin was precipitated by adding 20% H_2SO_4 dropwise until pH of 2 was reached. The lignin was vacuum-filtered and dried at 50°C for a few days.

Polyvinyl Alcohol (PVA) in (dimethyl sulfoxide) DMSO at 90°C were dissolved under magnetic stirring for three hours. Subsequently, lignin was blended into the PVA solution at 65°C and stirred for ten hours to ensure homogeneity. After cooling to room temperature, the solution was loaded into a 10 mL syringe fitted with a 21-gauge needle. The needle served as the electrode, while a rotating cylindrical collector (positioned opposite) enabled electrospinning at 16 kV. The solution was electrospun onto N-type silicon wafers at a controlled pumping rate of 0.6 mL/h.

The films were heat-treated in a nitrogen-purged tubular furnace. The temperature was first ramped from 25°C to 300°C at 5 °C/min, held for 5 minutes, then increased to 700°C at 10-15 °C/min for 3 hours before cooling to room temperature (Fig. 1).

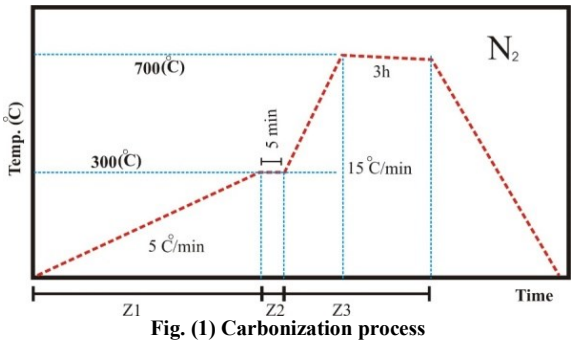

Fig. (1) Carbonization process

The structural properties of the films were analyzed using an X-ray diffractometer (XRD) employing CuKα radiation (1.5418Å) and an accelerated voltage of 40 kV. Crystallite size was estimated using the Williamson-Hall relation [10]

$$D_{hkl} = (A\lambda cos\theta . \beta_{hkl}) + (4\varepsilon sin\theta) \quad (1)$$

Where D_{hkl} (nm) is the crystallite size, A is a dimensionless shape factor (0.89), λ is the wavelength of the x-ray beam (nm), β_{hkl} is the full-width at half maximum (FWHM) of the diffraction peaks, ε is the strain, and θ (rad) is the diffraction angle

The molecular bonding and chemical composition of carbonized lignin/PVA:Fe_2O_3 films were investigated using Fourier-transform infrared (FTIR) spectroscopy.

The gas-sensing performance of films was tested using a custom-designed system (Fig. 2) with hydrogen (H_2), ammonia (NH_3), carbon dioxide (CO_2), and ethanol at various concentrations. The sensitivity (S%) was calculated as [12]:

$$S\% = \frac{\Delta R}{R_o} \times 100\% \quad (2)$$

where $\Delta R = |Ra - Rg|$ is the resistance difference between air (Ra) and the target gas (Rg). Furthermore, the response time (T_{res}) and recovery time (T_{rec}) were assessed. The response time is the amount of time needed for the sensor's resistance to reach 90% of its maximum change after exposure to the target gas (gas in), whereas T_{rec} is the amount of time needed for the sensor's resistance to return to 10% of its baseline after gas removal (gas out). Measurements were performed at ambient temperature and controlled humidity (10-50%), with 25% identified as optimal. Exposure and recovery times were fixed at 20 s after saturation/stabilization.

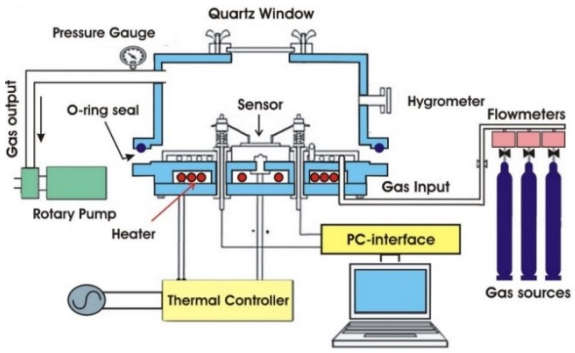

Fig. (2) A schematic diagram of the gas sensing system.

3. Result and Discussion

Figure (3) depicts the XRD pattern of Carbonized Lignin/PVA and Carbonized Lignin/PVA:Fe_2O_3 films. Carbonized lignin/PVA film show polycrystalline structure dominated by C_4 phase (hexagonal) and the presence of a trace amount of $C_6H_8O_4$ phase. C_4 phase is hexagonal in nature, evidenced by the observation of a (051) peak at 2θ = 68.89°, and have crystallite size of around 94 nm. Additionally, the $C_6H_8O_4$ phase is seen, overlaying the dominant C_4 phase. The $C_6H_8O_4$ phase shows 31% relative intensity to the C_4 peak, with a +0.18° peak shift, as depicted in Fig. (3a).

At 4 ppm Fe_2O_3, the C_{212} phase vanishes, while the C_4 phase intensifies (higher diffraction intensity). This enhancement is accompanied by a peak shift of approximately 0.4° to higher angles and an increase in crystallite size to about 99 nm, suggesting crystal growth within the dominant phase. Even at 5 ppm Fe_2O_3, the C_2H_4 phase is weakly indicated, whereas the C_4 phase still continues to be predominant. Again, the crystallite size increases to approximately 110 nm with a slight shift in the peak position in the higher angle direction. While at 7 ppm Fe_2O_3 level, the $C_{13}H$ phase begins to emerge, and the intensities of C_2H_4 and C_4 phases decrease. While reduced in intensity, the C_4 phase continues to be dominant, with a further peak shift to the lower angles and crystallite growth to 115 nm. Increasing the Fe_2O_3 concentration enhances phase evolution (disappearance of C_{212}, emergence of $C_2H_4/C_{13}H$) and enhances the crystallite growth of C_4.

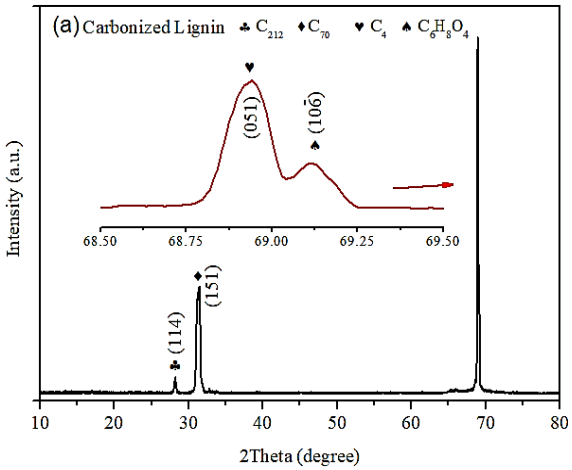

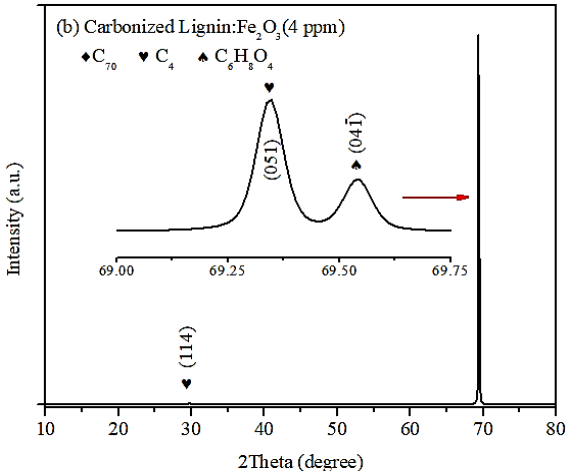

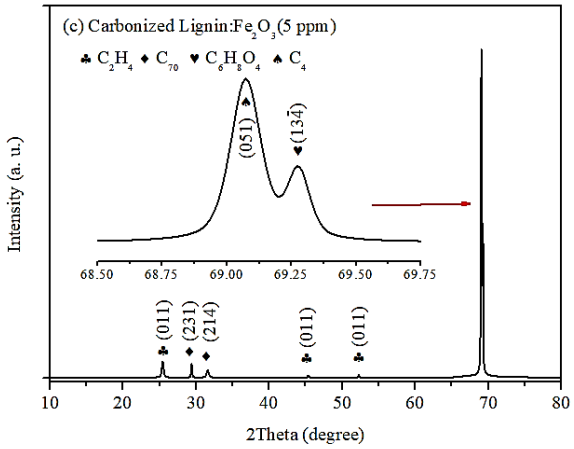

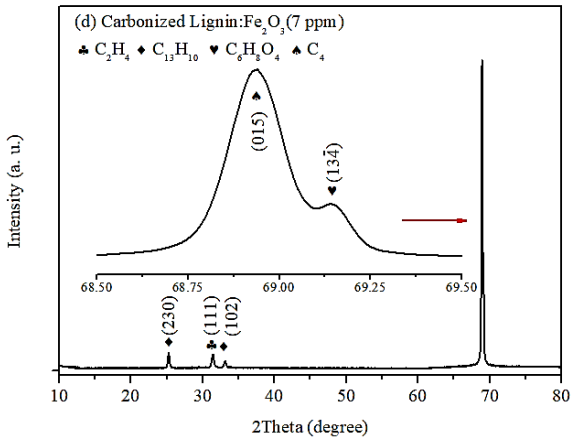

Fig. (3) XRD patterns of (a) the carbonized Lignin/PVA, (b, c, and d) the carbonized Lignin/PVA:Fe_2O_3 with Fe_2O_3 concentration of 4, 5, and 7 ppm, respectively

The C_4 diffraction peak shift and the crystallite size increase are caused by several factors, which include crystal growth and stress effects. The Fe_2O_3 nanoparticles provide nucleation, and this leads to crystallite size increase, which is controlled by crystal growth mechanisms. Stress effects primarily cause the shift of the C_4 peak to higher diffraction angles brought about by lattice parameter mismatch between the Lignin/PVA matrix and Fe_2O_3 nanoparticles. Lattice parameter mismatch generates compressive or tensile stresses in the crystal structure, as previously reported by Schwaminger et al. [13]. Thermal responses and phase changes also have significant roles in influencing structural changes. Fe_2O_3 particles affect the decompositions and crazing process of the lignin/PVA matrix, promoting a more ordered structural ordering. Fe_2O_3 catalyzes also phase transformation, resulting in the shifting of the diffraction peak position [14]. A third contributing factor is interfacial reactions, where the interaction between Fe_2O_3 nanoparticles and the micronized Lignin/polyvinyl alcohol matrix affects the electronic and structural characteristics of the composite [15].

The enhancement of the hydrogen content of the resulting phases and the appearance of hydrogenated

compounds (e.g., C_2H, $C_{13}H$, $C_{13}H_{10}$, and $C_6H_8O_4$) can be explained by various mechanisms.

The formation of hydrogen-rich compounds in the product led phases can be ascribed to various underlying reasons, which are. One of the significant factors is the catalytic action of Fe_2O_3 nanoparticles, resulting in abstraction and recombination of hydrogen, especially at high Fe_2O_3 concentrations. The process of carbonization decomposes complex organic molecules into low-hydrogen content intermediates, which recombine to produce hydrogen-rich phases [16,17]. Also, reduction reactions during carbonization, wherein the functionality of Fe_2O_3 as reactive species at high temperatures, also participate in the generation of hydrogen-rich hydrocarbon phases. At elevated temperatures, Fe_2O_3 can be reduced to metallic Fe or Fe_3O_4 and oxygen release generates a reducing environment that assists in the generation of hydrocarbons [18-20]. Also, high surface area of nanoparticles enhances adsorption and stabilization of hydrogen-containing molecules and becomes easier for them to be integrated into carbonaceous structures [21,22].

Figure (4) shows FE-SEM images of Lignin/PVA and Lignin/PVA:Fe_2O_3 films, showing sharp differences in morphology with increasing concentration of Fe_2O_3. Lignin/PVA films contained bulk aggregates of 187 nm and particles of 26 nm. Addition of 4 ppm Fe_2O_3 transformed spherical particles to nanorods (diameter = 29 nm, length = 112 nm). At 7 ppm Fe_2O_3, nanorods vanished, replaced by fibrous particles (45 nm diameter, 500 nm length) and irregular particles (56 nm diameter). Further increasing the concentration to 7 ppm led to the complete disappearance of nanorods and the development of fibrous-like particles with a diameter of 45 nm and length of approximately 500 nm, covered by irregular-shaped particles with an average diameter of 56 nm. Further increasing the concentration to 7 ppm led to the complete disappearance of nanorods and the development of fibrous-like particles with a diameter of 45 nm and length of approximately 500 nm, covered by irregular-shaped particles with an average diameter of 56 nm.

Nitrogen-assisted carbonization critically shaped the films' morphology. Carbonization tends to degrade organic components such as PVA and lignin to form a carbonaceous matrix. This enhances the structural stability and porosity of films and allows for the homogenous distribution of Fe_2O_3 nanoparticles within the carbonized matrix. Fe_2O_3 addition and carbonization synergistically drove morphological changes, i.e., the formation of nanorods, fibrous shape, and particle size reallocation. Results reflect the substantial influence of the amount of Fe_2O_3 and carbonization on the structure and morphology characteristics of the composite films.

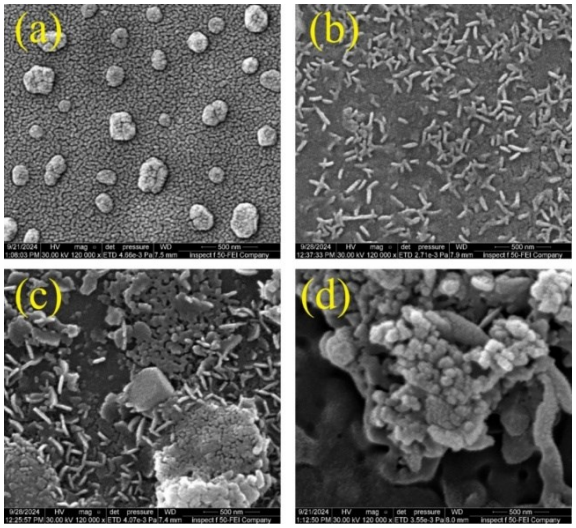

Fig. (4) FE-SEM images of (a) the carbonized Lignin/PVA, (b, c, and d) the carbonized Lignin/PVA:Fe_2O_3 with Fe_2O_3 concentration of 4, 5, and 7 ppm, respectively

Figure (5) shows the FTIR spectra in the range of 400-4000 cm^{-1} for carbon nanorods annealed at 600°C. When lignin is converted into carbon rods, the resulting. The FTIR spectrum reflects residual functional groups and chemical bonds present in the carbonized material. The broad peak at 3443 cm^{-1} arises from –OH stretching vibrations, attributed to residual moisture or surface hydroxyls from oxygen-containing groups that might still be present in the lignin and any remaining alcohol groups from solvent (ethanol). Furthermore, the nanorods absorb moisture from the environment due to their porous structure [23,24]. Carbonization significantly reduces the intensity of the –OH band. Peaks at 2923 and 2849 cm^{-1} are due to asymmetric/symmetric C–H stretching [25]. Carbonyl groups (C=O) peak at 1740 cm^{-1}. Its presence and intensity depend upon the oxidation level and retention of the functional groups during conversion of lignin to carbon [26]. The 1425 cm^{-1} band indicates aromatic C=C stretching and C–H deformation, confirming retained lignin aromaticity. Since lignin contains a lot of aromatic structures, carbon rods made from it should peak in this area, indicating that the aromatic structure was preserved during carbonization. The C–O stretch at 1117 cm^{-1} aligns with lignin's native ether/alcohol groups [27]. These peaks confirm oxygenated functional groups in the carbonized material. The sharp peak at 875 cm^{-1} corresponds to aromatic C–H out-of-plane bending (aromatic) common to either triazine or heptazine units within the structures, indicating the presence of aromatic rings in the carbon structure [28]. Peaks between 675-594 cm^{-1} arise from C–H stretching or hydrocarbon guest groups of hydrocarbon bonds or guest groups containing carbon and hydrogen [29].

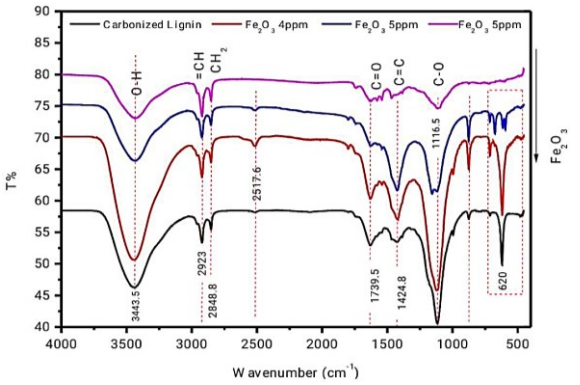

Fig. (5) FTIR spectra for the carbonized Lignin/PVA, and the carbonized Lignin/PVA:Fe_2O_3 with Fe_2O_3 concentration of 4, 5, and 7 ppm, respectively

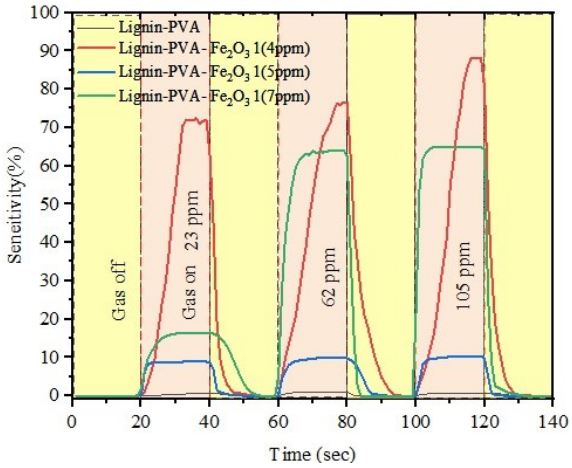

Fig. (6) Sensitivity of the fabricated films with different CO_2 concentrations

The sensitivity of carbonized lignin/PVA films to CO_2 gas concentrations of 23, 62, and 105 ppm and the effect of doping with Fe_2O_3 at concentrations of 4, 5, and 7 ppm, respectively, were tested. Carbonized lignin/PVA films did not initially show a significant response, this phenomenon can be attributed to an inadequate number of active sites available for robust CO_2 binding [30]. However, the addition of Fe_2O_3 at a concentration of 4 ppm significantly improved the sensitivity of the films (88%, 76%, and 72%) at CO_2 concentrations of 23, 62, and 105 ppm, respectively. In this case, CO_2 reacts with Fe_2O_3 to form siderite ($FeCO_3$), enabling reversible CO_2 storage [31,32]. The enhanced CO_2 absorption capacity of the films can be attributed to their morphological characteristics, which provide an increased surface area for gas interaction (Fig. 6). This structure enhances CO_2 adsorption via increased gas-solid contact. Conversely, films containing 5 ppm resulted in a decrease in sensitivity compared to their predecessors, although the increase did not exceed 10.4% with increasing gas concentration. In the same context, there is a slight increase (16%) in conjunction with the Fe_2O_3 concentration of 7 ppm, with a sudden increase and relative stability around 64.5% for the concentrations (62 and 105) ppm, as shown in Fig. (6a). Iron oxide concentration alters film morphology (FE-SEM, Fig. 4), which correlates with gas sensitivity changes. As evidenced by FE-SEM analysis, alterations in Fe_2O_3 concentration induce changes in particle size, porosity, and structural configuration. These modifications increase surface area, potentially improving gas adsorption and interaction with the target analyte (CO_2). The increased surface area provides additional active sites for gas exposure, which is critical for improving sensor responsiveness [33-36]. In addition, increasing the Fe_2O_3 concentration of Fe_2O_3 may cover or block the active sites on the fullerene rods or the carbonized lignin matrix. This reduces the available surface area for CO_2 adsorption, leading to decreased sensitivity [37].

To study the effect of operating temperature on the performance of the fabricated sensors, the sensors were additionally tested at 50°C and 100°C, as shown in Fig. (7). The carbonized lignin/PVA films showed no significant change at 50°C, but exhibited a sudden increase at 100°C. The nonlinear change in sensitivity may be attributed to the adsorption of surrounding water molecules (humidity), which blocks and disrupts the electrical conductivity pathways. This temperature may also anneal metastable defects, reducing the number of active sites for interaction with the target gas. When the operating temperature rises to a point where the water molecules previously trapped in the membrane are likely to evaporate, new functional groups such as carboxyl and carbonyl are introduced, or the edges of the carbon lattice are distorted, which act as new sensing sites, leading to the sudden increase in sensitivity [38].

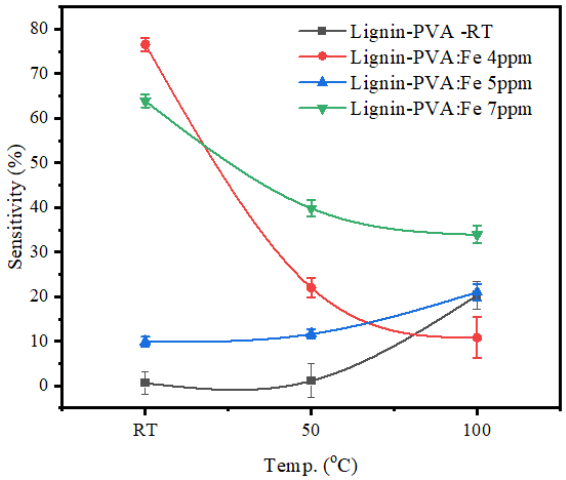

Fig. (7) Sensitivity of the fabricated films with different temperature

It was also observed that the sensitivity of 5 ppm films increased with the rise in operating temperature at the same rate as before, up to 21% at 100°C, while

the decrease in sensitivity values was observed for 4 and 7 ppm Fe_2O_3 films, as the sensitivity decreased to 22, 10.8% and 39.8, 33.9%, respectively.

At 100°C, thermal energy promotes the oxygen ion adsorption (O_2^-/O^-) on Fe_2O_3 surfaces for improving target gas molecule interactions. The 5 ppm Fe_2O_3 incorporated film exhibits optimum sensitivity as this amount optimizes effective oxygen ion adsorption while thermally lowering the activation energy barrier for surface reactions according to Arrhenius-type behavior [39,40]. Conversely, the 7 ppm Fe_2O_3 film displays a marked drop in sensitivity (from 39.8% to 33.9%), which can be traced to nanoparticle agglomeration or reduced active surface area as a result of excessive dopant loading. This is aligned with existing research where levels of Fe_2O_3 loading above 2 wt.% in activated carbon composites distorted the semiconductor matrix, lowering sensitivity even with increased analyte adsorption [41]. The 4 ppm Fe_2O_3 film is less sensitive (22% to 10.8%), which is indicative of a scarcity of catalytic sites for gas-surface chemistry. Undoped α-Fe_2O_3 films have also been found to be less sensitive towards baseline than the doped counterparts [42], and at 4 ppm, the diluted dispersion of Fe_2O_3 quashes catalysis even under thermal activation.

To ensure the selectivity of the films, the sensitivity of the films to H_2, NH_3 gases, CO_2 addition, and ethanol was tested. CO_2 was found to be superior, as the films did not show any regular response when exposed to the above gases.

4. Conclusion

Carbon nanorods were fabricated successfully from biomass-derived by-products obtained from palm-waste lignin. Fabrication of these nanostructures was a function of the optimal concentration of Fe_2O_3 as a catalytic additive, along with a carefully controlled carbonization process carried out under a nitrogen atmosphere. The structural and chemical properties of the lignin/PVA:Fe_2O_3 composite films were highly dependent on the interaction of Fe_2O_3. Also, CO_2 exposure considerably influenced the electrical conductivity of the carbonized lignin/PVA:Fe_2O_3 thin films, suggesting their potential application as a selective CO_2 sensing material.

References

[1] G. Kolumban-Antal et al., "A secure and portable multi-sensor module for distributed air pollution monitoring", *Sensors (Switzerland)*, 20 (2020) s20020403.

[2] S. Malik et al., "Nanomaterials-based biosensor and their applications: A review", *Heliyon,* 9 (2023) e19929.

[3] C. Li et al., "Review—Intracellular Sensors Based on Carbonaceous Nanomaterials: A Review", *J. Electrochem. Soc.,* 167 (2020) 037540.

[4] P. Simon and Y. Gogotsi, "Capacitive Energy Storage in Nanostructured Carbon–Electrolyte Systems", *Acc. Chem. Res.*, 46 (2013) 1094–1103.

[5] P. Bondavalli, P. Legagneux and D. Pribat, "Carbon nanotubes based transistors as gas sensors: State of the art and critical review", *Sens. Actuat. B Chem.,* 140 (2009) 304-318.

[6] S. Ganesan et al., "Microwave-assisted green synthesis of multi-functional carbon quantum dots as efficient fluorescence sensor for ultra-trace level monitoring of ammonia in environmental water", *Environ. Res.,* 206 (2022) 112589.

[7] S. Šafranko et al., "Preparation of multifunctional n-doped carbon quantum dots from citrus clementina peel: Investigating targeted pharmacological activities and the potential application for Fe^{3+} sensing", *Pharmaceut.,* 14 (2021) 090857.

[8] R. Yadav et al., "Lignin derived carbon fiber and nanofiber: Manufacturing and applications", *Compos. B Eng.*, 255 (2023) 110613.

[9] A.H. Ali et al., "Preparation and Performance Study of Lignin-Zinc Oxide Nanocomposite as a Lead Adsorbent", *Adv. J. Chem. A*, 8 (2025) 392-405.

[10] M.G. Suryanarayana and C. Norton, "Practical Aspects of X-Ray Diffraction", in: X-Ray Diffraction: A Practical Approach, Springer US, Boston (MA 1998), pp. 63–94.

[11] M.M. Alalousi et al., "Sensing Enhancement of Gold Nanoparticles Doped-TiO_2 Thin Films as H_2S Gas Sensor", *Nano Hybrids Compos.,* 35 (2022) 1-10.

[12] M. Lo Dayekh and S.A. Hussain, "Gas Sensor and Sensitivity, in: Metal-Oxide Gas Sensors", IntechOpen (2022).

[13] S.P. Schwaminger et al., "Iron Oxide Nanoparticles: Multiwall Carbon Nanotube Composite Materials for Batch or Chromatographic Biomolecule Separation", *Nanoscale Res. Lett.,* 16 (2021) 03491-5.

[14] P. Butnoi et al., "Electrospun nanocomposite fibers from lignin and iron oxide as supercapacitor material", *J. Mater. Res. Technol.,* 12 (2021) 2153-2167.

[15] A. Goldoni et al., "Advanced promising routes of carbon/metal oxides hybrids in sensors: A review", *Electrochim Acta*, 266 (2018) 139-150.

[16] R. Kumar et al., "Self-assembled nanostructures of 3D hierarchical faceted-iron oxide containing vertical carbon nanotubes on reduced graphene oxide hybrids for enhanced electromagnetic interface shielding", *Compos. B Eng.,* 168 (2019) 66–76.

[17] A. Bjelić et al., "Catalytic hydrogenation, hydrodeoxygenation, and hydrocracking processes of a lignin monomer model compound eugenol over magnetic Ru/C–Fe_2O_3 and mechanistic reaction microkinetics", *Catalysts,* 8 (2018) 100425.
[18] F. Schmalz et al., "Reaction path identification and validation from molecular dynamics simulations of hydrocarbon pyrolysis", *Int. J. Chem. Kinet.*, 56 (2024) 501-512.
[19] O.A. Hammadi, "Effects of Extraction Parameters on Particle Size of Iron Oxide Nanopowders Prepared by Physical Vapor Deposition Technique", *Iraqi J. Appl. Phys.,* 20(2B) (2024) 457-460.
[20] H.J. Mustafa, "Characterization and Comparison of Magnetite Nanoparticles Prepared by Coprecipitation and Autocombustion Techniques", *Iraqi J. Appl. Phys. Lett.*, 8(3) (2025) 885-88.
[21] Y. Hu et al., "Preparation and optical properties of magnetic carbon/iron oxide hybrid dots", *RSC Adv*., 7 (2017) 41304–41310.
[22] P.M. Cardoso, G.J. de Moreno and S.G. Pachuca, "Effect of Cobalt Dopants on Magneto-Optic Conversion of Magnetite Nanostructures", *Iraqi J. Appl. Phys. Lett.*, 8(1) (2025) 25-28.
[23] O. Derkacheva and D. Sukhov, "Investigation of lignins by FTIR spectroscopy", in: Macromol. Symp. (2008), pp. 61–68. DOI: 10.1002/masy.200850507.
[24] A. Singh et al., "Synthesis, characterization and performance of zinc ferrite nanorods for room temperature sensing applications", *J. Alloys Comp.*, 618 (2015) 475–483.
[25] J. Fu et al., "Study on the evolution pattern of the chemical structure of Fenton pretreated lignin during hydrothermal carbonization", *J. Enviro. Chem. Eng.,* 10 (2022) 107184.
[26] M. Song et al., "Alkali promoted the adsorption of toluene by adjusting the surface properties of lignin-derived carbon fibers", *Enviro. Sci. Pollut. Res.*, 26 (2019) 22284–22294.
[27] E. Stojanovska et al., "Developing and characterization of lignin-based fibrous nanocarbon electrodes for energy storage devices", *Compos. B Eng.*, 158 (2019) 239–248.
[28] A.B. Jorge et al., "H_2 and O_2 Evolution from Water Half-Splitting Reactions by Graphitic Carbon Nitride Materials", *The J. Phys. Chem. C,* 117 (2013) 7178–7185.
[29] J. Gan et al., "Lignocellulosic Biomass-Based Carbon Dots: Synthesis Processes, Properties, and Applications", *Small,* 19 (2023) 04066.
[30] W. Zhang et al., "Lignin derived carbon materials: current status and future trends", *Carbon Res.,* 1 (2022) 00009-1.
[31] A. Elhambakhsh, S. Heidari and P. Keshavarz, "Experimental Study of Carbon Dioxide Absorption by Fe_2O_3@glutamine/NMP Nanofluid", (2021), DOI: 10.21203/rs.3.rs-498743/v1.
[32] A. Fabozzi, F. Cerciello and O. Senneca, "Reduction of Iron Oxides for CO_2 Capture Materials", *Energies (Basel)*, 17 (2024) 071673.
[33] A. Zaker et al., "Carbon-based materials for CO2 capture: Their production, modification and performance", *J. Enviro. Chem. Eng.,* 11 (2023) 109741.
[34] X.Q. Zhang, W.C. Li and A.H. Lu, "Designed porous carbon materials for efficient CO_2 adsorption and separation", *New Carbon Materials*, 30 (2015) 481–501.
[35] U. Kamran and S.J. Park, "Chemically modified carbonaceous adsorbents for enhanced CO_2 capture: A review", *J. Clean Product.,* 290 (2021) 125776.
[36] M.E. Casco et al., "Effect of the porous structure in carbon materials for CO_2 capture at atmospheric and high-pressure", *Carbon,* 67 (2014) 230–235.
[37] F. Xu et al., "Green synthesis of magnetic mesoporous carbon from waste-lignin and its application as an efficient heterogeneous Fenton catalyst", *J. Clean Product.,* 285 (2021) 125363.
[38] M.-M. Titirici, "Hydrothermal Carbonisation: A Sustainable Alternative to Versatile Carbon Materials Habilitationsschrift", PhD thesis, University of Potsdam (2013).
[39] Y.R. Kumar et al., "A novel flexible CO_2 gas sensor based on polyvinyl alcohol/yttrium oxide nanocomposite films", *RSC Adv*., 14 (2024) 5022–5036.
[40] D. Tahir et al., "Enhanced Visible-Light Absorption of Fe_2O_3 Covered by Activated Carbon for Multifunctional Purposes: Tuning the Structural, Electronic, Optical, and Magnetic Properties", *ACS Omega*, 6 (2021) 28334-28346.
[41] R.M.T.D. Rajapaksha et al., "Enhancement of Gas Sensitivity of Ferric Oxide Thin Films by Adding Activated Carbon Nanoparticles", *Iconic Res. Eng. J.*, 4(10) (2021) 107-113.
[42] T.D. Rajapaksha et al., "Improvement of gas sensitivity of ferric oxide thin films by adding Mn nanoparticles", *Bull. Mater. Sci.,* 44 (2021) 182.

